

## Spectroscopic ellipsometry study of epitaxially grown $\text{Pb}(\text{Mg}_{1/3}\text{Nb}_{2/3})\text{O}_3\text{-PbTiO}_3/\text{MgO}/\text{TiN}/\text{Si}$ heterostructures

W. S. Tsang, K. Y. Chan, C. L. Mak,<sup>a)</sup> and K. H. Wong

Department of Applied Physics and Smart Materials Center, The Hong Kong Polytechnic University, Hung Hom, Hong Kong, China

(Received 21 April 2003; accepted 20 June 2003)

$0.65\text{Pb}(\text{Mg}_{1/3}\text{Nb}_{2/3})\text{O}_3\text{-}0.35\text{PbTiO}_3$  (PMN-PT) thin films have been grown on MgO/TiN-buffered Si(001) substrates using pulsed laser deposition. Their structural properties and surface morphology were examined by x-ray diffraction and scanning electron microscopy, respectively. All PMN-PT films grown at 670 °C show a cube-on-cube epitaxial relationship of PMN-PT(100)||MgO(100)||TiN(100)||Si(100). Discernable interfaces between layers in the heterostructures and crack-free surfaces are evident. A spectroscopic ellipsometer was used to study the optical characteristics of the films. It was revealed that the refractive index of the PMN-PT is  $\sim 2.50$  as measured at 635 nm. This value is only slightly less than that of the PMN-PT single crystal of 2.60. Our results suggest that the PMN-PT/MgO/TiN/Si heterostructure has an excellent potential for use in integrated optical waveguide devices. © 2003 American Institute of Physics. [DOI: 10.1063/1.1603339]

The unusual electro-optic properties of ferroelectrics coupled with the advances made in thin film fabrication technology in recent years allow thin-film ferroelectrics to be considered as the prime material candidate for many integrated optic devices. Potential applications include low-voltage electro-optic switching, compact low-threshold gain devices and second-harmonic generation.<sup>1</sup> Recently, thin-film  $\text{BaTiO}_3$  channel waveguides on single crystal MgO substrates have been fabricated.<sup>2,3</sup> An effective electro-optic coefficient of  $\sim 50 \pm 5$  pm/V has been achieved.<sup>2</sup> These  $\text{BaTiO}_3$  epitaxial structures form the basis of a highly confining guided wave electro-optic modulator that can operate at low voltage. Indeed, the basic design of such a device usually incorporates a ferroelectric film and a low refractive index buffer layer. Integrating these materials with silicon leads to devices on single integrated circuit chip. It is one of several strategies towards the realization of miniature optoelectronic circuits. At present, a fundamental issue in the development of this technology is to find appropriate ferroelectrics and buffer layer materials. Among various ferroelectrics for optical applications,  $0.65\text{Pb}(\text{Mg}_{1/3}\text{Nb}_{2/3})\text{O}_3\text{-}0.35\text{PbTiO}_3$  (PMN-PT) is one of the most promising ferroelectric candidates due to its extremely high electro-optics coefficient and strong photorefractive effect.<sup>4</sup> Indeed, PMN-PT has an electro-optic coefficient larger than the best value reported for  $(\text{Pb},\text{La})(\text{Zr},\text{Ti})\text{O}_3$  thin films.<sup>5</sup>

However, epitaxial PMN-PT cannot be grown directly on Si substrate due to a large lattice mismatch (the lattice constants of Si and PMN-PT are 0.543 and 0.402 nm, respectively). In order to overcome this problem, TiN and MgO are used as buffering layers between PMN-PT and Si in our studies. TiN has been known to grow epitaxially on Si via domain matching epitaxy.<sup>6</sup> Besides, TiN has many unique properties such as high electrical conductivity, high

chemical stability, and hardness. With such excellent properties, TiN is used as a buffer layer for integrating PMN-PT epitaxially on Si substrate. However, during deposition and postannealing of PMN-PT films, the high processing temperature and required ambient oxygen oxidize the TiN layer. As a remedial measure, a MgO buffer layer is laid on top to protect the TiN. Furthermore, the PMN-PT layer must be deposited on top of a material with a smaller refractive index in order to form a waveguide structure. Therefore, this MgO layer, with a much lower refractive index than PMN-PT, can produce a large refractive index difference and a strong beam confinement in a small space. This allows a very high intensity per unit power in the guide, and hence, a large nonlinear effect as well as a short interaction length.

PMN-PT/MgO/TiN heterostructures have been successfully grown on Si(001) substrates by *in situ* pulsed laser deposition using an ArF excimer laser. The 25.4 mm diameter and 5-mm-thick cylindrical  $0.65\text{PMN}\text{-}0.35\text{PT}$  target was homemade from single phase PMN-PT powder pressed at 80 MPa and sintered at 900 °C for 10 h. The MgO and TiN targets were sintered commercial targets with purities 99.9% and 99.5%, respectively. The Si substrates were ultrasonically cleaned in acetone first, followed by dipping into a 10% HF solution for 5 min to remove the native oxide layer. The target-to-substrate distance was kept at 40 mm. For the fabrication of TiN and MgO films, the pressure of the chamber was pumped down to  $5 \times 10^{-6}$  Torr. The substrate temperature was 650 °C. Laser running at 10 Hz repetition rate was properly focused to produce an on-target fluence of  $5 \text{ J/cm}^2$ . The typical layer thicknesses for TiN and MgO were about 150 and 100 nm, respectively. For the fabrication of PMN-PT films, deposition conditions of 6 Hz laser repetition rate,  $4 \text{ J/cm}^2$  energy density, 200 mTorr ambient oxygen pressure, and 670 °C substrate temperature were employed. All as-grown PMN-PT films were postannealed at the deposition temperature and pressure for another 10 min. Afterwards, the films were cooled naturally to room temperature.

<sup>a)</sup>Author to whom correspondence should be addressed; electronic mail: apaclmak@polyu.edu.hk

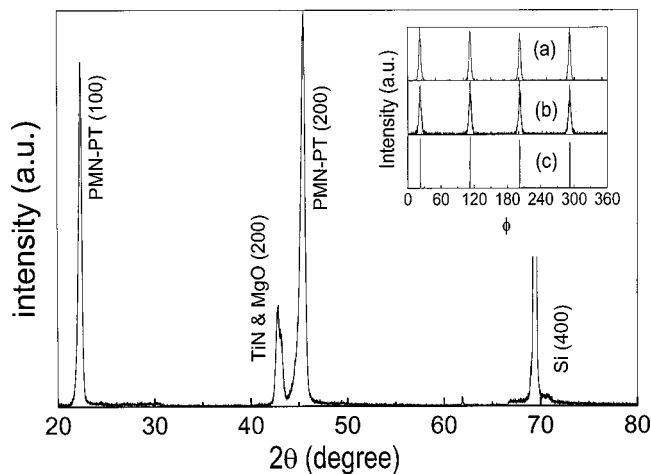


FIG. 1. The XRD  $\theta$ - $2\theta$  profile of the PMN-PT/MgO/TiN/Si. Inset shows the XRD  $\phi$  scans of the (a) PMN-PT(220), (b) MgO(200) and TiN(220), and (c) Si(220).

In order to obtain a particulate-free film, a shadow mask of  $5 \times 5 \text{ mm}^2$  was placed between the target and substrate to prevent particulates from reaching the surface of the substrate. The distance between the mask and the substrate was fixed at 15 mm.

The structural properties of the deposited films were characterized by a four-circle x-ray diffractometer with  $\text{Cu } K_\alpha$  radiation at an acceleration voltage of 50 kV.  $\theta$ - $2\theta$  scan was used to determine the crystal phase formed. The out-of-plane orientation was examined by  $\omega$  scan while the epitaxial growth of the films was confirmed using the  $360^\circ \phi$  scan. A scanning electron microscopy (SEM) was employed to examine the surface morphology of the films. The film thickness was deduced by measuring the cross section from the SEM micrographs. The optical properties of these heterostructures were studied by spectroscopic ellipsometry (SE). In our studies, the SE measurements were carried out at wavelengths between 450 and 830 nm with 5 nm intervals.

The x-ray diffraction (XRD)  $\theta$ - $2\theta$  profile of the PMN-PT/MgO/TiN/Si heterostructure is shown in Fig. 1. The lattice constants of TiN and MgO are 0.422 and 0.421 nm, respectively, hence, their x-ray diffraction peaks overlap with each other. Highly oriented single perovskite phase of PMN-PT films are observed. The lattice constant of the PMN-PT is  $\sim 4.02 \text{ nm}$ . The out-of-plane orientation of the PMN-PT(200) peaks was examined by  $\omega$  scan. The full width at half maximum (FWHM) of the rocking curve is  $1.36^\circ$ . This is larger than that of PMN-PT films grown on single crystal MgO (FWHM= $0.79^\circ$ ).<sup>7</sup> The XRD  $\phi$  scans of the PMN-PT(220), MgO(200), TiN(220), and Si(220) were performed to confirm the epitaxy of the grown films and the results are shown in the inset of Fig. 1. We notice that all diffraction peaks are at the same  $\phi$  angles and the peaks are separated by  $90^\circ$ . This indicates that the films are cube-on-cube grown on Si(100) substrate with epitaxial relationship of PMN-PT(100)||MgO(100)||TiN(100)||Si(100).

The surfaces of our PMN-PT films are, in general, very smooth. The grains are densely and regularly packed. No pores and weak links between irregular-shaped grains are observed. The rms surface roughness measured by atomic force microscope (AFM) is about 5.6 nm. From the cross-

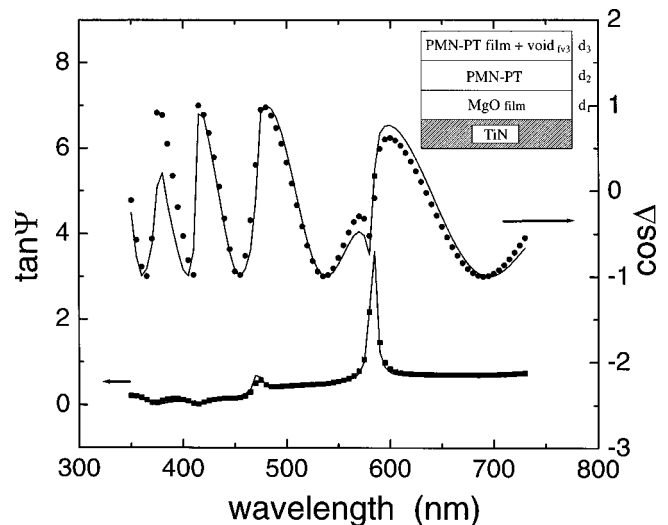


FIG. 2. The ellipsometric spectra of the heterostructure PMN-PT/MgO/TiN/Si. Inset shows the schematic structure of the four-layer model.

section micrograph (not shown), three discernable layers with columnar grain structures are observed. The thicknesses of PMN-PT, MgO, and TiN layers are estimated to be  $\sim 360$ , 90, and 160 nm, respectively.

The experimental and simulated ellipsometric spectra of the PMN-PT/MgO/TiN/Si heterostructure are shown in Fig. 2. Good agreement between the two spectra was obtained. In order to construct a credible computing model, the optical properties of each layer of TiN, MgO, and PMN-PT must be studied first. Ellipsometry spectrum of TiN film deposited on Si substrate was measured. The refractive index and extinction coefficient of such a single TiN layer were obtained directly. The optical properties of the TiN layer are metal-like, in which the values of  $n$  and  $k$  increase with wavelength. The estimated plasma energy (at which the real part of dielectric constant is equal to zero) is 2.41 eV, which is similar to the reported value.<sup>8</sup> When the frequency of light is below the plasma frequency, the propagation wave vector is purely imaginary. The transverse wave does not propagate in the medium and it is reflected at the interface. Even at 450 nm, the extinction coefficient is 0.6 and the skin depth of TiN is about 60 nm. All TiN layers in our samples are  $\sim 150 \text{ nm}$  thick. Consequently they can be treated as a semi-infinite bulk material and the reflection from Si substrate is neglected. Therefore, the PMN-PT/MgO/TiN/Si heterostructures are described by a four-layer model consisting a semi-infinite TiN layer, a thin MgO layer, a bottom bulk PMN-PT layer, and a surface layer that composed of bulk PMN-PT as well as voids of volume percentage  $f$ . These voids in the surface layer were mainly caused by surface roughness. The schematic structure is shown in the inset of Fig. 2. In order to describe the dispersion spectra for this surface PMN-PT layer, the Bruggeman effective medium approximation<sup>9</sup> was employed. In our fitting, the dispersion of the refractive indices of MgO and PMN-PT, similar to other oxygen-octahedral ferroelectrics, is expressed by a single term Sellmeier dispersion model<sup>10</sup> without absorption in the visible region

TABLE I. Fitting results based on dispersion model.

	$S_0(10^{14} \text{ m}^{-2})$	$\lambda_0$ (nm)	$d_1$ (nm)	$d_2$ (nm)	$d_3$ (nm)	$f$ (%)
MgO	$1.64 \pm 0.221$	$107.6 \pm 13.2$	$86.6 \pm 5.5$	—	—	—
PMN-PT	$1.00 \pm 0.013$	$216.6 \pm 10.3$	—	$361.7 \pm 14.4$	$5.5 \pm 1.3$	$78 \pm 13$

$$n^2(\lambda) - 1 = \frac{S_o \lambda_o^2}{1 - \left(\frac{\lambda_o}{\lambda}\right)^2}, \quad (1)$$

where  $S_o$  is the average oscillator strength and  $\lambda_o$  is the average oscillator position. Since the  $\text{BO}_6$  octahedral governs the lower lying conduction bands and the upper valence bands, the optical properties of oxygen-octahedral ferroelectrics are dominated by the  $\text{BO}_6$  octahedral. This lowest energy oscillator is the largest contributor to the dispersion of the refractive index. Other ions in the structure contribute to the higher-lying conduction band and have small effect on the optical properties. Because the band structure is similar in all the oxygen-octahedral, one oscillator formula can describe these dominated interband electronic transitions of these two bands. Based on this dispersion model, the fitting results are given in Table I. Comparing these thicknesses obtained in ellipsometry with those obtained from SEM, the agreement is very good to within 4%. For the surface roughness, the value obtained in ellipsometry is 5.5 nm ( $d_3$ ) which is consistent with that obtained by AFM (root mean square surface roughness=5.6 nm).

Figure 3 shows the refractive indices of MgO and PMN-PT layers. Obviously, the refractive index of MgO film grown on Si(001) substrates is smaller than that of single crystal (inset of Fig. 3). Similarly, the refractive index of PMN-PT grown on MgO/TiN buffered Si is smaller than that grown on single crystal MgO. The reduced refractive

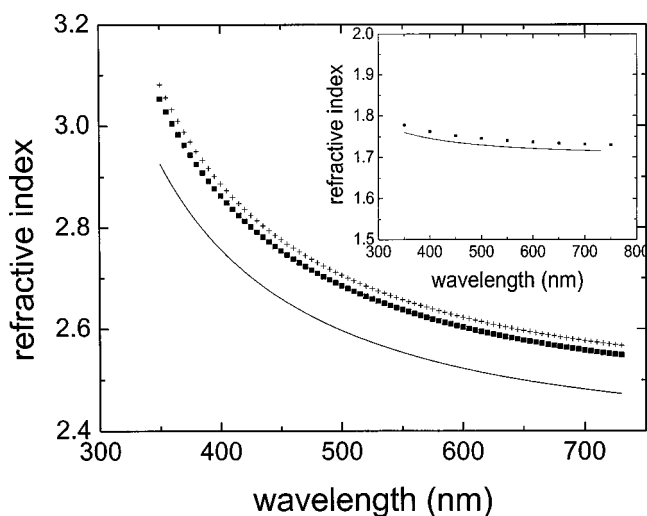


FIG. 3. The refractive indices of 0.65PMN-0.35PT single crystal (+), 0.65PMN-0.35PT films grown on single MgO crystal substrates (■), and on MgO/TiN buffered Si (—). Inset shows the refractive indices of MgO films from this study (—) and literature (■) (see Ref. 11).

indices are partly due to the poor crystallinity of the PMN-PT and MgO layers grown on Si substrates. This relationship is apparent if we compare the FWHM of rocking curves of PMN-PT(002) grown on MgO/TiN buffered Si (FWHM=1.39°) and on single crystal MgO (FWHM=0.79°). Furthermore, the surface roughness and particulates of the MgO layer increase the chance of developing voids into the PMN-PT film. This reduces the density of the PMN-PT films, and thus lowers their refractive indices. The SEM cross-section micrograph of the heterostructure, which shows the columnar growth feature, confirms this. Although the refractive indices of our PMN-PT layer are lower than those of single crystal, it is large enough to provide a large film/buffer layer refractive index difference ( $\Delta n \sim 0.8$  at 635 nm) that is important in producing highly confining guided wave.

In conclusion, for developing practical integrated optical devices, the integrated waveguide structure of PMN-PT/MgO/TiN/Si was fabricated. Our results show that the films are cube-on-cube grown on Si(100) with epitaxial relationship of PMN-PT(100)||MgO(100)||TiN(100)||Si(100). The optical properties of TiN are derived directly from the ellipsometric spectra and the refractive indices of MgO and PMN-PT films are described by Sellmeier model. The refractive index of PMN-PT films on MgO/TiN buffered Si at 635 nm is 2.50. This value is smaller than that grown on single crystal MgO. The poorer crystallinity and low density of the integrated PMN-PT films are responsible for the reduced refractive index. Nevertheless, the PMN-PT film/buffer layer index difference remains large enough to form good optical waveguides.

Part of this research was support by the Center for Smart Materials and a Research Grant of the Hong Kong Polytechnic University. W.S.T. and K.Y.C. were supported by MPhil studentships of the Hong Kong Polytechnic University.

- <sup>1</sup> Y. Xu, *Ferroelectric Materials and Their Applications* (North-Holland, Amsterdam, 1991).
- <sup>2</sup> D. M. Gill, C. W. Conrad, G. Ford, B. W. Wessels, and S. T. Ho, *Appl. Phys. Lett.* **71**, 1783 (1997).
- <sup>3</sup> A. Petraru, M. Siegert, M. Schmid, J. Schubert, and C. H. Buchal, *Mater. Res. Soc. Symp. Proc.* **688**, C8.1.1.
- <sup>4</sup> Y. H. Lu, J. J. Zheng, M. C. Golomb, F. L. Wang, H. Jiang, and J. Zhao, *Appl. Phys. Lett.* **74**, 3764 (1999).
- <sup>5</sup> H. Adachi, T. Mitsuyu, O. Yamazaki, and K. Wasa, *J. Appl. Phys.* **60**, 736 (1986).
- <sup>6</sup> T. Zheleva, K. Jagannadham, and J. Narayan, *J. Appl. Phys.* **75**, 860 (1994).
- <sup>7</sup> W. S. Tsang, MPhil thesis, The Hong Kong Polytechnic University.
- <sup>8</sup> J. H. Kang and K. J. Kim, *J. Appl. Phys.* **86**, 346 (1999).
- <sup>9</sup> D. A. G. Bruggeman, *Ann. Phys. (Leipzig)* **24**, 636 (1935).
- <sup>10</sup> M. DiDonenico, Jr. and S. H. Wemple, *J. Appl. Phys.* **40**, 720 (1969).
- <sup>11</sup> R. E. Stephens and I. H. Maalitsou, *J. Nat. Bur. Stand.* **49**, 249 (1951).